J Therm Anal Calorim (2011) 103:1111–1117
DOI 10.1007/s10973-010-1142-9

Synthesis, structural and thermal characterization of metaphosphatecobalt(II) salt

Trilochan Swain

Received: 16 September 2010 / Accepted: 27 October 2010 / Published online: 8 December 2010

Abstract A new inorganically template metaphosphate of Co(II) complex has been synthesized and characterized by different measurements such as DSC, FT-IR, C–H–N–O–S, ESR, TG-DTA and X-RD. Differential Scanning Calorimeter (DSC) elucidated negative specific heat of the system and has used to evaluate some thermo dynamical constants like activation energy (E_a), frequency factor (A), enthalpy and entropy of that system. The specific heat capacity of the system is measured both in atmospheric O_2 and N_2 atmosphere at different heating rates of 278, 283, 293 and 298 K min^{-1} in room atmosphere and 288 K min^{-1} in N_2 atmosphere.

Keywords X-RD · DSC · Negative specific heat capacity · Enthalpy · Entropy

Introduction

The preparation and structural chemistry of a number of organically template metal phosphates are extensively studied for their potential applications in many fields in the past few decades [1–6]. Some metal phosphites are reported for replacing metal phosphate [7–10]. The substitution of P(III) for P(V) is observed by Harrison et.al. In this case hydrogen phosphite group, $[HPO_3]^{2-}$, which is used as a new basic building block led to diversity of novel structures in organically templated metal phosphates. Many open-framework metal phosphites are synthesized like $[C_2H_{10}N_2]\cdot[V(HPO_3)_2]$, $[C_2H_{10}N_2]\cdot[Fe(HPO_3)_2]$ [11]; $[C_2H_{10}N_2]\cdot[Co_3(HPO_3)_4]$ [12]; $[C_2H_{10}N_2]\cdot[Cr(HPO_3)F_3]$[13]; $[C_2H_{10}N_2]\cdot[Mn_3(HPO_3)_4]$ [14]. However, using only metaphosphoric acid in the preparation of Co(II) complex is not synthesized till now apart from some organically template complexes. Here, I have evaluated the thermodynamic constants like activation energy, frequency factor, enthalpy, entropy and specific heat capacity of the complex at different heating rates of 283, 293 and 288 K min^{-1} (at N_2 atmosphere).

In all heating rates specific heat is found negative. The negative specific heat is an unusual phenomenon first discovered in statistical models of gravo-thermal collapse in globular clusters [15]. Motivated further by this fact, the study of specific heat beyond the weak-coupling limit has recently received considerable attention, in particular in view of the validity of the third law of thermodynamics [16–22]. Apart from fundamental thermodynamical questions, the study of specific heat in the quantum regime is also of interest because it can be related to entanglement properties [23]. Recently, two different methods towards the evaluation of a specific heat are proposed and discussed [16]. One possibility based on the thermal expectation value of the Hamiltonian describing the isolated system. Another approach, on which I have focused in this article, is widely used expression for the partition function of the dissipative system [16, 19, 25–32]. It is defined in terms of partition functions of the coupled system and of the uncoupled system.

$$Z = \frac{T_{r_{S+B}} e^{-\beta H}}{T_{r_B} e^{-\beta H_B}} \tag{1}$$

where the total Hamiltonian, $H = H_S + H_B + H_{SB}$, consisted of contributions from the system, bath and coupling between them. In the absence of coupling between system

Electronic supplementary material The online version of this article (doi:10.1007/s10973-010-1142-9) contains supplementary material, which is available to authorized users.

T. Swain (✉)
Indic Institute of Design & Research, Bhubaneswar, Orissa, India
e-mail: scienceorissa@rediffmail.com

and bath, Z reduces to the partition function of the system. Partition function (1) appears naturally in the Feynman–Vernon approach to dissipative systems [16] and can be related to the equilibrium properties of the system [33]. I have elucidated the origin of the negative specific heat for the case of entire system.

Experimental

In a typical synthesis for this compound, 7.03 g of $CoSO_4{\cdot}7H_2O$ and 2.56 g of metaphosphoric acid (60% HPO_3 + 40% $NaPO_3$) were dissolved in 25 cc of double distilled water. Both solutions were mixed at room temperature and stirred under ambient conditions until homogeneous. The stirred solution was left for 120 h. The resulting solution was neutralized to pH 7 by addition of alkali (0.1 N NaOH). The neutralized solution was stirred for 6 h under ambient conditions. Then it was left for 120 h. The resulting product was filtered, washed and dried in desiccators. Highly purified, deionized water was used in all solutions. Second distillation was carried out from alkaline $KMnO_4$ using an all-glass distillation apparatus.

Measurements

A varian E-112 X-band spectrometer was used for the measurement of EPR spectra of Co(II) species in solid state at SAIF, IIT-Bombay. An IR spectrum was obtained using a Thermo-Nicolet avtar 370 of solid sample. DSC measurements were performed on a Mettler Toledo, DSC 822 on 278,283, 293 and 298 K/min under atmospheric oxygen and 288 K/min on N_2 atmosphere. C–H–N analyser was performed on an Elementar systeme, vario EL III. Ir, DSC and C–H–N analyses were performed at ST & IC, Cochin University of Science and Technology, Cochin. Elemental analysis of O and S was performed at CDRI, Lucknow. X-ray crystallography measurement of powder sample was carried out at IIT, Gauhati. Thermogravimetric analysis (TG) and Differential thermal analysis (DTA) studied for the complex was made using Shimadzu DTG 50 (simultaneous DTA-TG) thermal analyser between 298 and 784 K using an aluminium crucible. pH measurements were performed using a Nucleonix type DP 301 digital pH meter equipped with combination of glass- Ag/AgCl/Cl^- (3 mol dm^{-3}NaCl) electrode. It was calibrated with standard buffers of pH 4.0, 7.0 and 9.0 (Merck).

Results and discussion

FT-IR analysis

The absence of peak at 504 cm^{-1}, which was present in metaphosphoric acid Ir spectrum, in Ir spectrum of complex revealed the presence of Co^{II}–O bond. This 504 cm^{-1} peak shifted to 534 cm^{-1}. The presence of 581 cm^{-1} peak indicated another type of Co^{II}–O bond. These two types of absorption bands are indicating the presence of two types of Co^{II}–O bond, i.e. high spin and low spin Co(II) metals that were also agreed with ESR spectrum. The peaks 843, 1030, 936, 976 and 1421 cm^{-1} were due to HPO deform, POH deform, P–O stretching, PO_2 s-stretching and PO_2 a-symmetric stretching, respectively. The peaks on 890 and 706 cm^{-1} are observed due to asymmetric and symmetric POP stretching vibrations, respectively. The peaks of 1061 and 1092 cm^{-1} are observed owing to asymmetric and symmetric stretching vibrations of O–P–O, respectively [34]. The broadened peak in the 3058–3168 cm^{-1} revealed due to P–H stretching vibrations. The band at 3446 cm^{-1} is observed due to intramolecular hydrogen bonding of –OH bond.

Elemental analysis

The elemental analysis of the bulk product was also consistence with the theoretical values. Anal. Calcd. For complex $\{Co^{II}_{10}(Na_{16}P_{20}O_{60}H_{60})(H_2O)_8\}(SO_4)_2{\cdot}4H_2O$ is H:2.79%, S:2.12%, O:42.58% found H:2.8, S:2.12% and O:41.80%.

Magnetic analysis

Electron Paramagnetic Resonance (EPR) spectrum data of complex viz. $g_{\|}$, $g_{\perp}$ and g_{av} were 2.6, 1.62 and 1.95, respectively. $g_{\|} > g_{\perp}$ is obtained from this complex. The magnetic moment μ_S (in B.M.) is found 5.03 and 1.402. The 5.03 B.M. magnetic moment indicated the presence of some Co^{II} metal in high spin state. The experimental magnetic moment, μ_{exp} (1.402 B.M.), is found less than μ_S (3.87 B.M.). This indicated the presence of some low spin octahedral Co^{II} metals.

TG-DTA spectra

From TG analysis, the mass loss as temperature increased from 426 to 494 K was 17.52% (calc. 17.52 ± 0.35%). At this temperature 16 sodium, 84 Hydrogen and 2 sulphur were removed from sample. Within experimental temperature range (690 K), mass loss was 20.14% (calc. 20.14 ± 0.31). In this temperature range, all the above elements including 5 oxygen were removed from sample. The TG-DTA spectrum is figured in Fig. 1. From DTA spectrum, the reaction is found exothermic in nature which was observed to be similar with DSC spectra.

Crystal structure analysis

To determine the crystal structure of cobalt compound X-ray diffraction, data are collected at room temperature

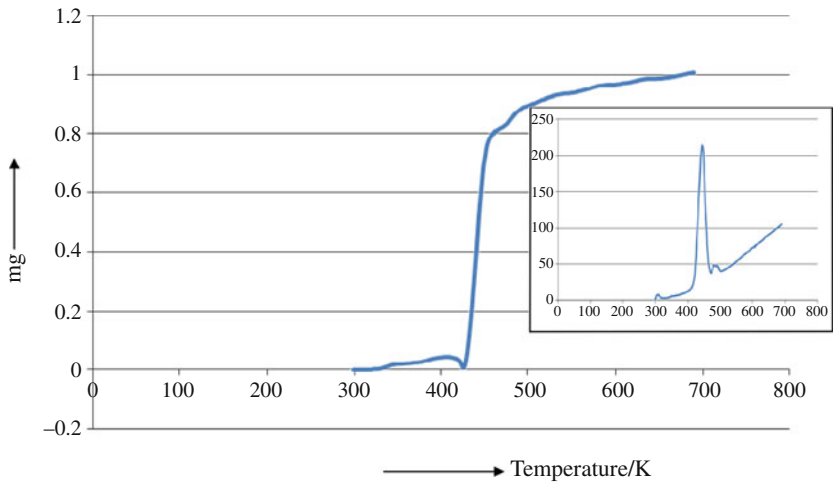

Fig. 1 TG-DTA spectrum of complex

with graphite-monochromated MoK_α radiation on an XPERT PRO diffractometer operating in $\omega/2\theta$ scan mode. The cell parameters are determined from a least-squares refinement of 15 centred reflections. Crystal data and experimental details of the title compound are collected in Table 1. The X-RD spectrum of complex is figured in Fig. 2.

The monoclinic unit cell contained four molecules of ($Co_{10}Na_{16}P_{20}O_{80}H_{84}S_2$). In the coordination sphere of Co^{II}, axial and equatorial bond lengths of Co–O bond were 2.066 and 2.174 Å, respectively [35, 36]. Axially bond lengths of plane O–Co–O are observed at 4.356 Å and this plane was obtained at an angle of 10.272°. The axial bond length of plane Co–O–H is observed 3.168 Å and made an angle of 14.002°. The bond length of O–Na is found 2.422 Å and made an angle of 18.622°. The bond length of Co–O–Na plane is observed 4.490 Å and made an angle of 9.817°. The bond distance of P atom to the O atom was 1.546 Å which is in good agreement with the study of Sharma et al. and Hua et al. [37]. The bond distance of plane O–P–O was 3.092 Å and made an angle of 14.517°. The bond length of hydrogen bonded plane of above molecule was O–P–O–H 4.067 Å and made an angle of 11.007°. The total distance of PO_3^{3-} plane was 4.638 Å and made an angle of 9.527°. The distance of Co^{II} bonded of above plane $Co(PO_3)^{2-}$ was 6.698 Å and made an angle of 6.642°. The total distance of H–P–O plane was 2.916 Å and made an angle of 15.167°. When H atom bonded with P atom through O atom, the distance of plane, P–O–H, was 2.536 Å and made an angle of 17.852°. The equatorial Co^{II} bond length of chain, Co–O–P–O–P, is found 6.686 Å and made an angle of 6.642°. The numerical values of this pattern are listed in Table 2.

Table 1 Crystal data and experimental details of the title compound

Empirical formula	$Co_5Na_8P_{10}O_{40}H_{42}S$
Molecular mass/g	3006
Temperature/K	298
Wavelength/Å	1.542475
Unit cell dimensions/Å	
$a = 13.43$ (1)	
$b = 5.424$ (7)	$\beta = 98.2$ (1)
$c = 10.92$ (1)	
Volume/Å^3	795.46(7)
Z	4
Crystal colour	Purple
Theta range for data collection/°	5.005–99.995
Number of points	9500
Scan axis	Gonio
Scan step size	0.01
Time per step	0.5
Scan type	Continuous
$K\alpha_2/K\alpha_1$	0.5
h k l	0 0 0

Differential scanning calorimeter

From Eq. 1, one obtained by means of standard thermodynamic relations a specific heat [19]

$$C = k_\beta \beta^2 \frac{\partial^2}{\partial \beta^2} \ln(Z) \tag{2}$$

Here, k_B is the Boltzmann constant and the temperature T appears $\beta = 1/k_B T$. In the following, I assumed the removal particle to consist of harmonic oscillators and the coupling to be bilinear in complex and removal coordinates. In order to elucidate the appearance of negative specific heat (2), it was sufficient to consider a stylized minimal model where the remove particle consisted of only a single degree of freedom described by the Hamiltonian.

$$H_R = \frac{P^2}{2m} + \frac{f_R}{2} q^2 \tag{3}$$

where, f_R denotes the spring constant.

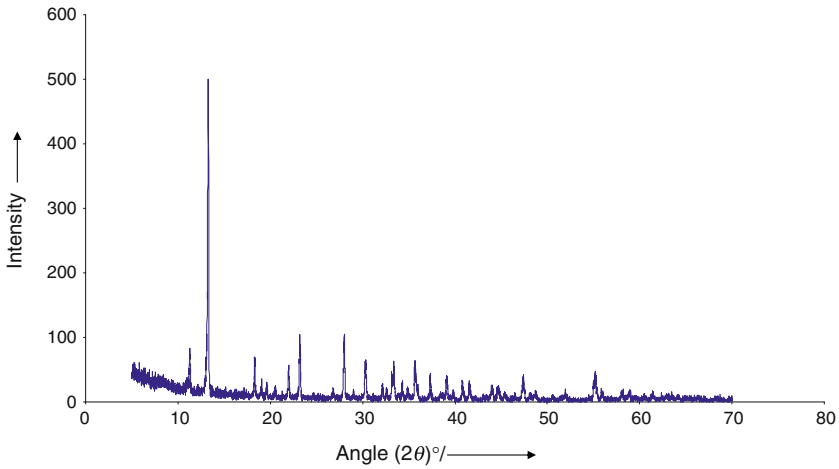

Fig. 2 X-RD spectrum of complex

Table 2 X-ray powder diffraction numerical values and pattern of cobalt compound (Fig. 2)

Peak no	2θ/°	d-value/Å	I/I_o
1	11.275	7.8537	16.6
2	13.285	6.6716	100
3	18.295	4.8536	13.8
4	19.055	4.6600	7.2
5	19.635	4.5233	6.2
6	20.545	4.3255	6.2
7	22.015	4.0400	5.0
8	23.195	3.8364	11.0
9	26.845	3.3228	20.8
10	28.005	3.1882	21.0
11	29.035	3.0775	4.0
12	30.335	2.9481	13.0
13	32.155	2.7852	5.6
14	32.625	2.7465	4.0
15	33.395	2.6844	12.6
16	34.315	2.6152	6.0
17	34.905	2.5716	4.2
18	35.705	2.5162	12.8
19	37.325	2.4101	8.8
20	39.135	2.3028	8.0
21	40.785	2.2134	6.8
22	41.555	2.1743	6.6
23	43.995	2.0593	5.2
24	44.755	2.0258	5.0
25	47.435	1.9174	8.4
26	55.225	1.6643	9.4

The complex governed by the Hamiltonian

$$H_C = \frac{P^2}{2M} + \frac{f_C}{2}Q^2 \tag{4}$$

Both in the cases of free particle, oxidation (O_2) and Nitrogenation (N_2) (spring constant $f_C = 0$) and of a harmonic oscillator ($f_C > 0$), the coupling Hamiltonian is given by

$$H_{CR} = -f_R qQ + \frac{f_R}{2}Q^2 \tag{5}$$

The mass of a single remove particle oscillator was "m". This removal particle coupled with complex having mass "M" harmonically. In my analysis a free particle (O_2 or N_2) was in contact with the single degree of freedom environment described by Eqs. 3 and 5. Complex and removal particles are assumed to stay in thermal equilibrium with each other at the inverse temperature β. Hence, the density matrix of the total system is given by a Gibb's state.

$$\rho_{CR} = Z_{CR}^{-1} \exp[-\beta(H_C + H_R + H_{CR})] \tag{6}$$

where, $Z_{CR} = T_r \exp[-\beta(H_C + H_R + H_{CR})]$ denotes the partition function of the total system.

The partition function $Z_R = T_r \exp[-\beta H_R]$ of the removal particle's degree of freedom is given by

$$Z_R = \frac{1}{2\sin\left(\frac{\hbar\beta\omega_o}{2}\right)} \tag{7}$$

where,

$$\omega_o^2 = \left(\frac{f_R}{m}\right) \tag{8}$$

ω_o was the frequency of remove particle oscillator. From Eq. 2 the specific heat capacity of this removal particles are given below.

$$C_R = k_B g\left(\frac{\hbar\beta\omega_o}{2}\right) \tag{9}$$

where,

$$g(x) = (x/\sin x)^2$$

In order to obtain a well-defined partition function for the free particle, I restricted its motion to a region of inside the system. The system is supposed to be sufficiently large

such that the energy level spacing can be neglected in compared with the thermal energy k_BT [19]. Under this condition the space of the system will turn out to be irrelevant in the sequel.

The frequency of underdamped complex ($\varsigma < 1$)

$$\omega = \omega_0\{\zeta \pm (\zeta^2 - 1)^{\frac{1}{2}}\}$$

ς is called as damping ratio. In this case the complex loses energy along with removal particles and return to the thermally stable state.

The specific heat capacity of complex is given below.

$$C_C = k_B g\left(\frac{\hbar\beta\omega}{2}\right)$$

The total heat capacity of the system is given below.

$$C = C_C + C_R = -k_B g\left(\frac{\hbar\beta\omega}{2}\right) + k_B g\left(\frac{\hbar\beta\omega_o}{2}\right)$$

Since, damping ratio <1, the specific heat capacity of the complex was negative. Hence, the specific heat capacity of the total system was negative.

The experimental molar heat capacities for sample are listed in Table 3. The experimental molar heat capacity is fitted in a polynomial equation with temperature. The entropy is calculated from $C_p \ln T$. The fraction of mass loss at each temperature is subtracted from total mass of sample for calculation of specific heat capacity, enthalpy and entropy. Activation energy and frequency factor are calculated from Arrhenius equation by plotting $\ln k$ versus $1/T$.

$$\ln k = \ln A - \frac{E_a}{RT}$$

where, k specific heat capacity at each temperature and A frequency factor.

The polynomial equation for specific heat capacity, enthalpy and entropy is given below.

$$Y\{(C_p), (H_T - H_{298}), (S_T - S_{298})\} = a_nT^n + a_{n-1}T^{n-1} + \cdots + a_2T^2 + a_1T + C$$

The values of $a_1, a_2, \ldots, a_n$ and C are tabulated in Tables S1 and S2. These tables can be published as supplementary materials.

Table 3 Total heat evolve and onset temperature of each heating rate

Heating rate/ K min^{-1}	Heat evolve/J g^{-1}	Onset temperature/K
278	−622.93	441.25
283	−602.00	455.43
293	−597.66	448.44
298	−594.00	458.73
288 (N_2 atmosphere)	−185.89	457.65

Heating rate—283 K min^{-1}

At the heating rate of 283 K min^{-1}, all experimentally calculated specific heat capacity are found negative, 300–474 K, due to damping ratio <1. In temperature range 300–372 K, specific heat capacity was negative with the increase in temperature. The specific heat capacity suddenly increased in negative value with the increase in temperature from 456 to 464 K. This large negative value was due to rapid loss of mass at above temperature ranges. The mass of sample slightly increased due to occurrence of slow oxidation at temperature ranges 466–474 K.

The activation energy, E_a, and frequency factor, A, from temperature of onset to peak were 14.64 kJ mol^{-1} and 8737 K^{-1}, respectively.

Heating rate—293 K min^{-1}

At heating rate of 293 K min^{-1}, all experimentally calculated specific heat capacities were negative, 300–406 K, due to damping ratio <1. In temperature range 300–390 K, specific heat capacity decreased in negative value in increase of temperature and further increased from 396 to 406 K. The specific heat capacity having less negative value, which might be due to rate of oxidation, was greater than rate of mass loss. The specific heat capacity suddenly increased in negative value with the increase in temperature from 450 to 465.33 K. This large negative value was due to rapid loss of mass at above temperature ranges. The positive value of specific heat capacity, 466 to 478 K, which might be due to rapid rate of oxidation (mass of sample increases by addition of oxygen during oxidation), was greater than rate of mass loss. As a result of which damping ratio was >1.

The activation energy, E_a, and frequency factor, A, from temperature of onset to peak were 7.96 kJ mol^{-1} and 1583 K^{-1}, respectively.

Heating rate—288 K min^{-1} (At N_2 atmosphere)

At the heating rate of 288 K min^{-1} in atmospheric N_2, all experimentally calculated specific heat capacity are found negative, 300–358 K, due to damping ratio <1. At temperature range 300–358 K, the specific heat capacity was negative value in increase of temperature. In temperature range 360–396 K, specific heat capacity suddenly increased in negative value with the increase in temperature and further increased from 402 to 430 K. The specific heat capacity was negative with the increase in temperature from 432 to 454 K. Again specific heat capacity suddenly increased in negative value with the increase in temperature from 456 to 468 K. This large negative value was due to rapid loss of mass at above temperature ranges. The

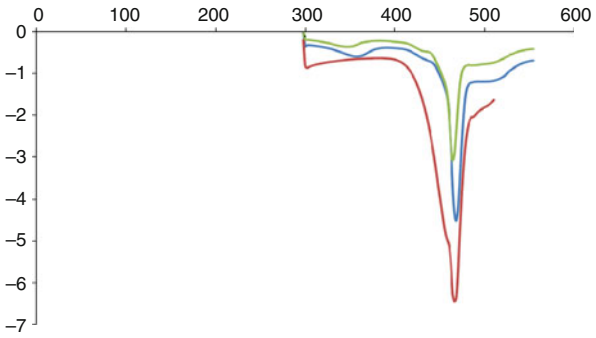

Fig. 3 DSC spectra of complex at 293 K min^{-1} (*upper*), 288 K min^{-1} (*middle*; N_2 atmosphere) and 283 K min^{-1} (*bottom*) from which negative specific heat was evaluated

negative specific heat capacity above peak temperature, mass of sample continued to decrease due to no oxidation in N_2 atmosphere, increased in temperature range 470–478 K (See Fig. 3).

The activation energy, E_a, and frequency factor, A, from temperature of onset to peak were 14.22 kJ mol^{-1} and 4194 K^{-1}, respectively.

The total heat evolved and onset temperature of each heating rate is tabulated in Table S3. The Table S3 can be published as supplementary materials. The total heat evolved decreased with the increase in heating rate.

Conclusions

A new inorganically template metaphosphate of Co(II) complex synthesized and characterized by different measurements is mainly of thermo dynamical character. The specific heat capacity of sample was found negative. After peak temperature, due to slow oxidation of sample, mass of sample slightly increased. Hence, specific heat capacity is observed less negative. In the case of nitrogen atmosphere, the mass of sample declined even after peak temperature due to no oxidation. The specific heat capacity is found more negative.

Acknowledgements The author (TS) thanks Department of chemistry, Utkal University for providing necessary facility for TG-DTA experiment of complex.

References

1. Cao G, Hong H, Mallouk TE. Layered metal phosphates and phosphonates: from crystals to monolayers. Acc Chem Res. 1992;25:420–7.
2. Feng S, Xu R. New materials in hydrothermal synthesis. Acc Chem Res. 2001;34:239–47.
3. Clearfield A, Sharma CVK, Zhang B. Crystal engineered supramolecular metal phosphonates: crown ethers and iminodiacetates. Chem Mater. 2001;13:3099–112.
4. Lohse DL, Sevov SC. $Co_2(O_3P–CH_2–PO_3)·H_2O$: a novel microporous diphosphonate with an inorganic framework and hydrocarbon-lined hydrophobic channels. Angew Chem Int Ed Engl. 1997;36:1619–21.
5. Serre C, Ferey G. Hydrothermal synthesis and structure determination from powder data of new three-dimensional titanium(IV) diphosphonates $Ti(O_3P–(CH_2)_n–PO_3)$ or MIL-25_n ($n = 2$, 3). Inorg Chem. 2001;40:5350–3.
6. Soghomonian V, Chen Q, Haushalter RC, Zubieta J. Investigations into the targeted design of solids: hydrothermal synthesis and structures of one-, two-, and three-dimensional phases of the oxovanadium–organodiphosphonate system. Angew Chem Int Ed Engl. 1995;34:223–6.
7. Rodgers JA, Harrison WTA. Ethylenediamine zinc hydrogen phosphite, $[H_2N(CH_2)_2NH_2]_{0.5}·ZnHPO_3$, containing two independent, interpenetrating, mixed inorganic/organic networks. Chem Commun 2000;2385–86.
8. Harrison WTA, Phillips MLF, Nenoff TM. $(CN_3H_6)_2·Zn(HPO_3)_2$: an open-framework zincophosphite built up from polyhedral 12-rings. Dalton Trans 2001;2459–61.
9. Lin ZE, Zhang J, Zheng ST, Yang GY. Synthesis and characterization of a novel open-framework nickel–zinc phosphite with intersecting three-dimensional 16-ring channels. J Mater Chem. 2004;14:1652–5.
10. Gordon LE, Harrison WTA. Amino acid templating of inorganic networks: synthesis and structure of L-asparagine zinc phosphite, $C_4N_2O_3H_8·ZnHPO_3$. Inorg Chem. 2004;43:1808–9.
11. Fernandez S, Pizarro JL, Mesa JL, Lezama L, Arriortua MI, Olazcuaga R, Rojo T. Two new three-dimensional vanadium(III) and iron(III) phosphites templated by ethylenediamine: $(C_2H_{10}N_2)_{0.5}[M(HPO_3)_2]$. Ab initio structure determination, spectroscopic, and magnetic properties. Chem mater. 2002;14: 2300–7.
12. Fernandez S, Pizarro JL, Mesa JL, Lezama L, Arriortua MI, Rojo T. Hydrothermal synthesis of a new layered inorganic–organic hybrid cobalt(II) phosphite: $(C_2H_{10}N_2)[Co_3(HPO_3)_4]$: crystal structure and spectroscopic and magnetic properties. Int J Inorg Mater. 2001;3:331–6.
13. Fernandez S, Pizarro JL, Mesa JL, Lezama L, Arriortua MI, Rojo T. $(C_2H_{10}N_2)[Cr(HPO_3)F_3]$: the first organically templated fluorochromium(III) phosphite. Angew Chem Int Ed Engl. 2002; 41:3683–5.
14. Fernandez S, Pizarro JL, Mesa JL, Lezama L, Arriortua MI, Olazcuaga R, Rojo T. A new layered inorganic–organic hybrid manganese(II) phosphite: $(C_2H_{10}N_2)[Mn_3(HPO_3)_4]$. Hydrothermal synthesis, crystal structure, and spectroscopic and magnetic properties. Chem Mater. 2000;12:2092–8.
15. Lynden-Bell D, Wood R. The gravo-thermal catastrophe in isothermal spheres and the onset of red-giant structure for stellar systems. Mon Not R Astr Soc. 1968;138:495–525.
16. Hanggi P, Ingold G-L. Quantum Brownian motion and the third law of thermodynamics. Acta Phys Pol B. 2006;37:1537–50.
17. Horhammer C, Buttner H. Information and entropy in quantum Brownian motion thermodynamic entropy versus von Neumann entropy. J Stat Phys. 2008;133:1161–74.
18. Bandyopadhyay M. Quantum thermodynamics of a charged magneto-oscillator coupled to a heat bath. J Stat Mech Theory Exp 2009; doi:10.1088/1742-5468/2009/05/P05002.
19. Hanggi P, Ingold G-L, Talkner P. Finite quantum dissipation: the challenge of obtaining specific heat. New J Phys 2008; doi: 10.1088/1367-2630/10/11/115008.
20. Wang C-Y, Bao J-D. The third law of quantum thermodynamics in the presence of anomalous couplings. Chin Phys Lett. 2008;25: 429–32.

21. Kumar J, Sreeram PA, Dattagupta S. Low-temperature thermodynamics in the context of dissipative diamagnetism. Phys Rev E 2009; doi:10.1103/PhysRevE.79.021130.
22. Ingold G-L, Hanggi P, Talkner P. Specific heat anomalies of open quantum systems. 2009; doi:10.1103/PhysRevE.79.061105.
23. Wiesniak M, Vedral V, Brukner C. Heat capacity as an indicator of entanglement. Phys Rev B 2008; doi:10.1103/PhysRevB.78.064108.
24. Feynman RP, Vernon FL. The theory of a general quantum system interacting with a linear dissipative system. Ann Phys (N.Y.). 1963;24:118–73.
25. Caldena AO, Leggett AJ. Quantum tunnelling in a dissipative system. Ann Phys (N.Y.). 1983;149:374–456.
26. Grabert H, weiss U, Talkner P. Quantum theory of the damped harmonic oscillator. Z Phys B. 1984;55:87–94.
27. Leggett AJ, Chakravarty S, Dorsey AT, Fisher MPA, Garg A, Zwerger W. Dynamics of the dissipative two-state system. Rev Mod Phys. 1987;59:1–85.
28. Grabert H, Schramm P, Ingold G-L. Quantum Brownian motion: the functional integral approach. Phys Rep. 1988;168:115–207.
29. Ford GW, Lewis JT, Connell REO. Quantum oscillator in a blackbody radiation field II. Direct calculation of the energy using the fluctuation-dissipation theorem. Ann Phys (N.Y.). 1988; 185:270–83.
30. Hanke A, Zwerger W. Density of states of a damped quantum oscillator. Phys Rev E. 1995;52:6875–8.
31. Dittrich T, Hanggi P, Ingold G-L, Kramer B, Schon G, Zwerger W. Quantum transport and dissipation Chap. 4. New York: Wiley; 1998.
32. Ford GW, Connell REO. Quantum thermodynamic functions for an oscillator coupled to a heat bath. Phys Rev B 2007; doi: 10.1103/PhysRevB.75.134301.
33. Ingold G-L. Path integrals and their application to dissipative quantum systems. Lect Notes Phys 611. Berlin: Springer; 2002. p. 1.
34. Zhang D, Yue H, Shi Z, Feng S. Hydrothermal synthesis and structural characterization of organically templated zincophosphites: $[C_6H_{22}N_4]_{0.5}[Zn_2(HPO_3)_3]$ and $[C_3N_2H_5][Zn_{1.5}(HPO_3)_2]$. Solid State Sci. 2005;7:1256–60.
35. Calligaris M, Nardin G, Randaccio L, Ripamonti A. Structural aspects of the synthetic oxygen-carrier *NN*-ethylenebis-(salicylideneiminato)cobalt(II): structure of the addition compound with oxygen containing dimethylformamide. J Chem Soc A 1970; 1069–74.
36. Meyer W, Biedermann K, Gubo M, Hammer L, Heinz K. Superstructure in the termination of CoO(111) surfaces: low-energy electron diffraction and scanning tunneling microscopy. Phys Rev B 2009; doi:10.1103/PhysRevB.79.121403.
37. Sharma R, Sharma RP, Bala R, Quiros M, Salas JM. A trinuclear cobalt(III) phosphate complex with a novel molecular structure: synthesis and crystal structure of $\{[Co(en)_2]_3(PO_4)(HPO_4)\}_2(H_2PO_4)Cl_7{\cdot}6H_2O$. Inorg Chem Commun. 2006;9:782–4.